Flavoenzymes at the crossroads of biocatalysis and structural biology

Nguyen, Quoc-Thai

Publication date:
2017

4

Discovery and characterization of an F_{420}-dependent glucose-6-phosphate dehydrogenase from *Rhodococcus jostii* RHA1

Quoc-Thai Nguyen, Gianluca Trinco, Claudia Binda, Andrea Mattevi and
Marco W. Fraaije

Cofactor F_{420}, a 5-deazaflavin involved in obligatory hydride transfer, is widely distributed among archaeal methanogens and actinomycetes. Owing to the low redox potential of the cofactor, F_{420}-dependent enzymes play a pivotal role in central catabolic pathways and xenobiotic degradation processes in these organisms. A physiologically essential deazaflavoenzyme is the F_{420}-dependent glucose-6-phosphate dehydrogenase (FGD), which catalyzes the reaction F_{420} + glucose-6-phosphate $\rightarrow$ $F_{420}H_2$ + 6-phosphogluconolactone. Thereby, FGDs generates the reduced F_{420} cofactor required for numerous $F_{420}H_2$-dependent reductases, involved e.g., in the bioreductive activation of the antitubercular prodrugs pretonamid and delamanid. We report here the identification, production, and characterization of three FGDs from Rhodococcus jostii RHA1 (Rh-FGDs), being the first experimental evidence of F_{420}-dependent enzymes in this bacterium. The crystal structure of Rh-FGD1 has also been determined at 1.5 Å resolution, showing a high similarity with FGD from Mycobacterium tuberculosis (Mtb-FGD1). The cofactor-binding pocket and active-site catalytic residues are largely conserved in Rh-FGD1 compared with Mtb-FGD1, except for an extremely flexible insertion region capping the active site at the C-terminal end of the TIM-barrel, which also markedly differs from other structurally related proteins. The role of the three positively charged residues (Lys197, Lys258, and Arg282) constituting the binding site of the substrate phosphate moiety was experimentally corroborated by means of mutagenesis study. The biochemical and structural data presented here provide

the first step towards tailoring Rh-FGD1 into a more economical biocatalyst, e.g., an F_{420}-dependent glucose dehydrogenase that requires a cheaper co-substrate and can better match the demands for the growing applications of $F_{420}H_2$-dependent reductases in industry and bioremediation.

4

4.1. Introduction

The unusual cofactor F_{420}, a 7,8-didemethyl-8-hydroxy-5-deazariboflavin, was originally discovered in various archaea (Cheeseman et al. 1972) (Figure 4.1). It was demonstrated that in both methanogenic and non-methanogenic archaea, F_{420} represents a central catabolic redox cofactor involved in the oxidation of energy sources (e.g., H_2 and formate) (Jacobson et al. 1982; Vitt et al. 2014; Tzeng et al. 1975a; Wood et al. 2003) and the reduction of cofactors such as $NADP^+$ and tetrahydromethanopterin (Tzeng et al. 1975b; Warkentin et al. 2001; Hartzell et al. 1985; Aufhammer et al. 2005). In recent years, it has become clear by genome sequence analyses and biochemical studies that the deazaflavin cofactor is also utilized by numerous enzymes in actinobacteria, including *Mycobacterium tuberculosis* (Mtb)—the notorious causative agent of tuberculosis (Daniels et al. 1985). In actinomycetes, F_{420} was found to be involved in several important processes such as biosynthesis of antibiotics in *Streptomyces* spp. (e.g., tetracycline, lincosamide, aminoglycoside) (Wang et al. 2013; Coats et al. 1989; Li et al. 2009a), degradation of coumarin derivatives (e.g., carcinogenic aflatoxins) (Taylor et al. 2010; Lapalikar et al. 2012b; Ahmed et al. 2015) and other aromatic compounds (e.g., picrate and related compounds) (Ebert et al. 1999; Heiss et al. 2002; Jirapanjawat et al. 2016). For mycobacteria, there is a compelling evidence that F_{420} is essential to render the bacilli persistent in hostile and challenging environments, such as anaerobic conditions, and oxidative and nitrosative stress (Hasan et al. 2010; Gurumurthy et al. 2013; Purwantini and Mukhopadhyay 2009). Interestingly, in vivo activation of the novel antitubercular nitroimidazole prodrugs—such as pretomanid (PA-824), delamanid (OPC-67683), and TBA-354—strictly requires a selective reduction of these prodrugs facilitated by an $F_{420}H_2$-dependent reductase (Stover et al. 2000; Matsumoto et al. 2006; Denny 2015). Owing to the newly discovered mode of action, these nitroimidazole compounds are highly promising as they exhibit no cross-resistance with the current front-line antitubercular drugs in vitro and even exert activity on non-replicating tubercle bacilli (Stover et al. 2000; Matsumoto et al. 2006; Singh et al. 2008). Delamanid (OPC-67683) was recently clinically approved for multidrug-resistant tuberculosis whereas pretomanid (PA-824) and TBA-354 are currently in phase III and phase I clinical trials, respectively (Tasneen et al. 2015).

The discovery of this novel antimycobacterial class of drugs is attracting an increasing interest in F_{420}-dependent enzyme research (Taylor et al. 2013). Due to the unique redox potential (−340 mV) of F_{420}, which is lower than that of FAD (−220 mV) and even of the classical hydrogen carrier $NAD(P)^+$ (Jacobson and Walsh 1984; de Poorter et al. 2005), $F_{420}H_2$-dependent enzymes are capable of catalyzing hydrogenation of a wide range of organic compounds which are otherwise recalcitrant to reductive activation such as enones (Taylor et al. 2010; Lapalikar et al. 2012b; Lapalikar et al. 2012a) and imines (Coats et al. 1989; Li et al. 2009a; Li et al. 2009b) in various heterocycles (Schrittwieser et al. 2015). These enzymes thus hold the promise of being highly valuable in industrial biotechnology, bioremediation, and can be exploited as a complement to the available toolboxes for asymmetric chemical synthesis (Taylor et al. 2013; Greening et al. 2016; Ney et al. 2016).

4
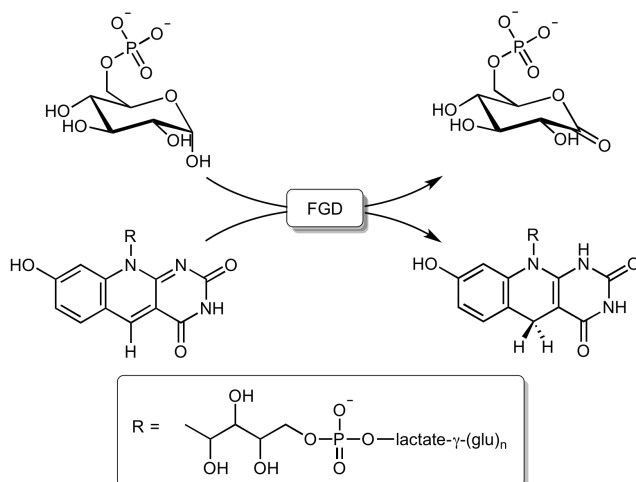
Figure 4.1: Reaction catalyzed by F_{420}-dependent dehydrogenase (FGD). Glucose-6-phosphate is oxidized into 6-phosphogluconolactone by FGD concomitantly with the formation of the reduced F_{420} coenzyme, which is subsequently employed by various $F_{420}H_2$-dependent reductases.

As most bacterial F_{420}-dependent enzymes are involved in catalyzing reductions, several F_{420}-dependent dehydrogenases have evolved with the purpose to maintain a cytosolic reservoir of reduced F_{420} ($F_{420}H_2$). In mycobacteria and other actinomycetes, glucose-6-phosphate dehydrogenases (FGDs) seem to be the main producer of $F_{420}H_2$, by catalyzing the reaction F_{420} + glucose-6-phosphate $\rightarrow$ $F_{420}H_2$ + 6-phosphogluconolactone (Figure 4.1). FGD was first identified in *Mycobacterium smegmatis* and subsequently in other actinomycetes, including Mtb (Purwantini and Daniels 1996; Purwantini et al. 1997; Purwantini and Daniels 1998). Since the identification of the first FGD two decades ago in Daniels' lab (Purwantini and Daniels 1996), only two FGDs from actinomycetes, namely *M. smegmatis* and Mtb, have been characterized in detail (Bashiri et al. 2007; Bashiri et al. 2010). These two FGDs share 37% sequence similarity and belong to an F_{420}-dependent enzyme subgroup within the luciferase-like hydride transferase family. The affinity of both enzymes for F_{420} and glucose-6-phosphate (G6P) falls in a comparable range, facilitating the release of the resulting reduced cofactor to be consequently exploited by downstream $F_{420}H_2$-dependent enzymes. Heterologous expression in *Escherichia coli* of both FGDs was found to be troublesome, often resulting in formation of inclusion bodies. Structural characterization of an FGD from Mtb has been recently described (Bashiri et al. 2008).

Rhodococci are high G+C content, Gram-positive aerobic, non-sporulating actinomycetes of high biotechnological and environmental importance due to their ability to catalyze an array of unique enzymatic reactions (van der Geize and Dijkhuizen 2004). A recent bioinformatic study suggested that *Rhodococcus jostii* RHA1 is among the actinomycetes that carry the largest number of F_{420}-dependent enzymes. It was predicted to possess at least 104 deazaflavoenzymes

Table 4.1: List of primers used in this study. The mutation sites were indicated as underlined oligonucleotides.

fgd genes	Forward primers (5′–3′)	Reverse primer (5′–3′)
RHA1_RS43115 (Rh-FGD1)	ATGGTGATCAAGTTCGGGTAC	TCATGCGAGCCCTCGCAG
RHA1_RS10755 (Rh-FGD2)	CTACCCCCGCAGCCG	ATGGCCCACGAACTCAAGC
RHA1_RS43570 (Rh-FGD3)	ATGACACAGCAGTTAAAGCTC	TCAGCCCAGGGCACG
RHA1_RS43115-K197N	TACAACTCCATGCC(ATT)ACCGGACGTGCAGATG	CATCTGCACGTCCGGT<u>AAT</u>GGCATGGAGTTGTA
RHA1_RS43115-K258N	TGACACCGGAGCAG<u>AAT</u>CATTCGATCGACGATC	GATCGTCGATCGAATG<u>ATT</u>CTGCTCCGGTGTCA
RHA1_RS43115-R282Q	CAGGTGGCGAAG<u>CAG</u>TGGATCGTGGCG	CGCCACGATCCA<u>CTG</u>CTTCGCCACCTG

(Selengut and Haft 2010). Nevertheless, up to date there is no experimental evidence for the presence of deazaflavoenzymes in *R. jostii* RHA1. Therefore, in this work we aimed to: 1) verify the existence of FGDs in *R. jostii* RHA1 (Rh-FGD) by heterologous expression of putative FGD-encoding genes in *E. coli*; 2) characterize the catalytic properties of the identified enzyme(s); and 3) obtain and analyze the crystal structure of a Rh-FGD.

4.2. Experimental section

4.2.1. Expression and purification of Rh-FGD1 in *E. coli*

R. jostii RHA1 was grown in Lysogeny Broth (LB) at 30 °C after which genomic DNA was extracted using the GenElute Bacterial Genomic DNA kit from Sigma. Three putative *fgd* genes, RHA1_RS43115, RHA1_RS10755, and RHA1_RS435-70, were amplified from *R. jostii* RHA1 genomic DNA using Phusion High-Fidelity DNA polymerase (Thermo Scientific) and the corresponding pairs of primers as listed in Table 4.1. The purified PCR products (100–200 ng) were treated with 0.5 U Taq polymerase (Roche) and 0.75 mM dATP by incubation at 72 °C for 15 min to introduce the 3′-A overhangs. The resulting insert DNA fragments were ligated into the pET-SUMO vector according to the instruction manual of the Champion pET SUMO expression system (Invitrogen). The construction of the Rh-FGD1 mutants K197N, K258N, R282Q was done by using the QuikChange® mutagenesis method with primers (Table 4.1) designed by the web-based QuikChange® Primer Design Tool (Agilent Technologies) and the pET-SUMO-RHA1_RS43115 plasmid as template. All constructs were confirmed by sequencing.

Proteins were initially expressed in *E. coli* BL21(DE3), grown in Terrific broth containing 50 μg/mL kanamycin, 1% (w/v) glucose and induced with 1 mM isopropyl β-D-1-thiogalactopyranoside (IPTG) at 24 °C when the cells reached OD600 ∼0.7–0.8. To overcome the insolubility of the overexpressed proteins in *E. coli* BL21(DE3), the expression hosts were changed to *E. coli* C41(DE3) (Lucigen) for both the wild-type and mutant Rh-FGDs. The culture conditions were kept the same as for *E. coli* BL21(DE3), except for the addition of 0.2% (w/v) glucose. The cells were grown until late stationary phase and harvested by centrifugation at 4600 × g for 10 min (Beckman–Coulter JA-10 rotor, 4 °C). Cells

4

were resuspended in lysis buffer (50 mM KPi pH 7.8, 400 mM NaCl, 100 mM KCl, 10% (v/v) glycerol, 1 mM β-mercaptoethanol, 20 mM imidazole) and disrupted by sonication using a VCX130 Vibra-Cell (Sonics & Materials, Inc., Newtown, USA) at 4 °C (5 sec on, 10 sec off, 70% amplitude, total of 5 min). Following centrifugation at 20000 × g for 45 min (Beckman–Coulter JA-25.5 rotor, 4 °C) to remove unbroken bacteria and cellular debris, the supernatant was applied onto a 5-mL HisTrap HP column (GE Healthcare) pre-equilibrated in the same buffer. The recombinant enzyme with the His-SUMO tag was eluted with a gradient from 20–500 mM imidazole in the same buffer. Fractions containing the pure enzyme as indicated by SDS-PAGE and FGD activity assay were pooled, desalted to remove imidazole, and concentrated in a 30-kDa MWCO Amicon (Milipore) centrifugal filter unit. Protein concentration was estimated using the Waddell's method (Waddell 1956).

To obtain the native enzyme, the His-SUMO tag was cleaved by incubating with 1% (mol/mol) SUMO protease (Invitrogen) for 2 h at 4 °C. The His-SUMO tag, uncleaved protein, and SUMO protease were removed by applying the cleavage mixture onto a second HisTrap column. The native enzyme was concentrated and finally purified through a Superdex 200 10/300 GL (GE Healthcare) in 10 mM HEPES pH 7.5, 100 mM NaCl, 10% (v/v) glycerol, 1 mM β-mercaptoethanol prior to crystallization experiments.

4.2.2. Thermostability

Analysis of Rh-FGD1 thermostability was based on the unfolding temperature, Tm, determined by the use of the Thermofluor® technique (Pantoliano et al. 2001) with a Bio-Rad C1000 Touch Thermal Cycler (Bio-rad Laboratories, Inc.) in 96-well plates. Each well had a final volume of 25 µL containing 1.6 µM Rh-FGD, 5 × SYPRO Orange (Invitrogen), buffers and/or additives. The protein start buffer was exchanged to 50 mM KPi pH 7.8, 150 mM NaCl for the buffer screen and to 50 mM KPi pH 7.8, 500 mM NaCl, 100 mM KCl for the additive screen. The compositions of the buffers and additives are described in Boivin et al. (Boivin et al. 2013).

4.2.3. Spectrophotometric assay for FGD activity

FGD activity was routinely monitored by following the reduction of F_{420} at 420 nm, 25 °C, pH 7.5 using an absorption coefficient ε_{420} of 41.4 mM^{-1} cm^{-1} (Eirich et al. 1978; Purwantini et al. 1992) in a V-650 spectrophotometer from Jasco (IJsselstein, The Netherlands). F_{420} was isolated from M. smegmatis as previously described (Bashiri et al. 2010; Isabelle et al. 2002) (*M. smegmatis* mc^2 4517 and the plasmid pYUBDuet-FbiABC were kind gifts from Dr. G. Bashiri, the University of Auckland, New Zealand). The assay mixture typically contained 50 mM Tris/HCl pH 7.5, 300 mM NaCl, 1 mM β-mercaptoethanol, 1 mM EDTA, 100 nM enzyme, 20 µM F_{420}, 1 mM glucose-6-phosphate (G6P) in a final volume of 500 µL. For steady-state kinetics, 10 nM enzyme was used in the same buffer except for the experiments with glucose that were performed with 500 nM enzyme. Kinetic data were analyzed using non-linear regression to the Michealis–Menten equation using GraphPad Prism v. 6.0 (GraphPad Software Inc., La Jolla, CA, USA). For the pH optima determination, the reactions contained 40 mM Britton-Robinson

buffer (Britton and Robinson 1931), 100 nM enzyme, 20 µM F_{420} and were initiated by adding 1 mM G6P. In the experiments, enzyme activity was monitored at 401 nm (an isosbestic point of F_{420}; $\varepsilon_{401} = 25$ mM^{-1} cm^{-1}) (Jacobson et al. 1982; DiMarco et al. 1990) for 5 min.

4.2.4. Substrate profiling

Alternative phosphate-sugar substrates for FGD were screened in a SynergyMX microplate spectrophotometer (BioTek) using 96-well plates with clear bottom. The reaction mix (200 µL) contained 100 nm enzyme, 10 mM substrate, and 29.6 µM F_{420} in the same buffer as described in the general spectrophotometric assay. The tested compounds for substrate profiling were: D-glucose, D-mannose-6-phosphate, D-fructose-6-phosphate, α-D-glucose-1-phosphate, α-D-galactose-1-phosphate, and D-glucosamine-6-phosphate. The absorbance of F_{420} at 420 nm was monitored in intervals of 45 sec for 1 h.

4.2.5. Crystallization, X-ray data collection, and structural determination of Rh-FGD1

Native Rh-FGD1 crystals were obtained using the sitting-drop vapour diffusion technique at 20 °C by mixing equal volumes of 9.0 mg/mL protein in 10 mM HEPES pH 7.5, 10% (v/v) glycerol, 100 mM NaCl, 1 mM β-mercaptoethanol and of the mother liquor containing 0.16 M ammonium sulfate, 0.08 M sodium acetate pH 4.6, 20% (w/v) PEG 4000, 20% (v/v) glycerol. X-ray diffraction data were collected at the PXI and PXIII beamlines of the Swiss Light Synchrotron in Villigen, Switzerland (SLS) and at the ID23-1 beamline of the European Synchrotron Radiation Facility in Grenoble, France (ESRF). Image integration and data scaling were processed with MOSFLM (Battye et al. 2011) and programs of the CCP4 suite (Winn et al. 2011). Detailed data processing statistics are shown in Table 4.2. The Rh-FGD1 structure was initially solved by molecular replacement using MOLREP (Vagin and Teplyakov 2010) using the coordinates of FGD1 from *M. tuberculosis* (PDB ID code 3B4Y) (Bashiri et al. 2008) as the search model devoid of all ligands and water molecules. Model building and structure analysis was carried out with COOT (Emsley and Cowtan 2004) whereas alternating cycles of refinement was performed with Refmac5 (Murshudov et al. 1997). Figures were created by CCP4mg (McNicholas et al. 2011); atomic coordinates and structure factors were deposited in the Protein Data Bank under the PDB ID code 5LXE.

4.3. Results

4.3.1. Expression and purification of Rh-FGDs in *E. coli*

Three genes encoding putative homologs of Mtb-FGD (accession number KBJ-40183) (Bashiri et al. 2007; Bashiri et al. 2008) were identified by BLAST: RHA1_RS43115 (WP_011600337.1), RHA1_RS10755 (WP_011595003.1), and RHA1_RS43570 (WP_011600440.1) (with 84, 84, and 83% sequence identity to Mtb-FGD1, respectively). These genes were amplified from *R. jostii* RHA1 genomic DNA, cloned into the pET-SUMO vector and expressed in *E. coli* C41(DE3) as N-terminal SUMO-hexahistidine fused proteins using IPTG as an inducer. The

4

cultivation conditions were optimized for the production of the soluble and active proteins, resulting in 48-hour growth at 24 °C with 1 mM IPTG in Terrific Broth as the most effective condition. By testing the cell extracts containing all three different proteins (RHA1_RS43115, RHA1_RS10755, and RHA1_RS43570 referred to as Rh-FGD1, Rh-FGD2, and Rh-FGD3, respectively), it was found that they all exhibit FGD activity. Rh-FGD1 and Rh-FGD2 exhibited comparable specific activity whereas Rh-FGD3 was >20-fold less active. We focused our exploration on the best expressed FGD, namely Rh-FGD1. Typically, approximately 80 mg of pure Rh-FGD1 was obtained from 1 L of TB culture. Furthermore, it is worth noting that Rh-FGD1 is flanked by genes putatively encoding a 6-phosphogluconate dehydrogenase and a glucose-6-phosphate isomerase. This strongly suggests that Rh-FGD1 is indeed a glucose-6-phosphate dehydrogenase.

4.3.2. pH optimum and thermostability

Rh-FGD1 displayed an optimum for activity on glucose-6-phosphate at pH 7.5–8.0 (Figure 4.2). This is somewhat similar to the FGDs from Mtb [6.5–7.0 (Bashiri et al. 2008)] and from *M. smegmatis* [two separate pH optima: 6.0 and 8.0 (Pur-

Table 4.2: Data collection and refinement statistics

PDB ID code	5LXE
Space group	$P2_1$
Resolution (Å)	1.47
a, b, c (Å)	81.4, 88.1, 88.8
R_{sym}[a,b] (%)	5.0 (55.0)
Completeness[b] (%)	98.7 (96.9)
Unique reflections	106774
Multiplicity[b]	3.9 (3.1)
I/σ[b]	10.9 (1.7)
CC$_{1/2}$	0.99 (0.70)
Number of atoms:	
—protein	4933
—sulfate, glycerol, water	$2 \times 5, 2 \times 6, 571$
Average B value for all atoms (Å^2)	25
R_{cryst}[b,c] (%)	16.2 (27.1)
R_{free}[b,c] (%)	18.5 (25.1)
Rms bond length (Å)	0.021
Rms bond angles (°)	2.02
Ramachandran outliers (%)	0

[a]$R_{\mathrm{sym}} = \sum |I_i - \langle I \rangle| / \sum I_i$, where I_i is the intensity of ith observation and $\langle I \rangle$ is the mean intensity of the reflection.
[b]Values in parentheses are for reflections in the highest resolution shell.
[c]$R_{\mathrm{cryst}} = |F_{obs} - F_{calc}| / |F_{obs}|$ where F_{obs} and F_{calc} are the observed and calculated structure factor amplitudes, respectively. R_{cryst} and R_{free} were calculated using the working and test sets, respectively.
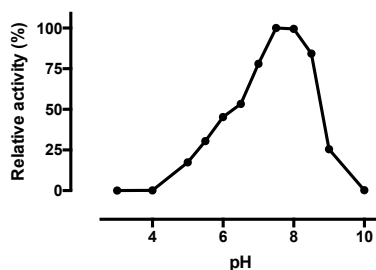
Figure 4.2: Effect of pH on Rh-FGD1 activity. The reaction contains 40 mM Britton–Robinson buffer, 100 nm Rh-FGD1, 20 μM F_{420}, and 1.0 mM G6P and activity was monitored by following the absorbance at 401 nm (isosbestic point of F_{420}) for 300 sec at 25 °C.

wantini and Daniels 1996)]. For further studies on Rh-FGD1, pH 7.5 was chosen to monitor FGD activity.

The thermostability of Rh-FGD1 was evaluated by determining apparent melting temperatures (T_m) using the Thermofluor technique (Pantoliano et al. 2001). This revealed that Rh-FGD1 represents a stable enzyme, exhibiting T_m values above 35 °C in most common buffer systems (Figure 4.3). The best stabilizing buffers were HEPES, citrate, and phosphate. Several additives were found to have significant effects on the thermostability of Rh-FGD1. NaCl, glycerol, and divalent cations (e.g., Mg^{2+}, Ca^{2+}, and Mn^{2+}) exerted marked effects, resulting in T_m values of above 55 °C. The stabilizing effect of NaCl depends greatly on its concentration: an increase in NaCl concentration from 50 mM to 1 M (in either HEPES or Tris/HCl) drastically elevates the T_m by around 20 °C. Based on these findings, we typically stored Rh-FGD1 in a phosphate-based buffer with both NaCl and glycerol as additives. Remarkably, the enzyme can retain >90% its activity after one year when being stored at −80 °C.

4.3.3. Substrate profiling and steady-state kinetics

Rh-FGD1 is strictly dependent on F_{420} as coenzyme. The enzyme did not show any significant activity when NAD^+, $NADP^+$, FAD, or FMN was used as alternative electron acceptors. Rh-FGD1 was also found to be highly specific for G6P as electron donor. All tested alternative phosphate-sugars displayed significantly lower activity when compared to G6P. 10 mM D-mannose-6-phosphate, D-fructose-6-phosphate, D-glucosamine-6-phosphate reached only 1.1, 4.8, and 2.8% of the rate obtained with 1 mM G6P, respectively. The free anomeric carbon C1 of the sugar is crucial for the dehydrogenation as no detectable FGD activity was observed with α-D-glucose-1-phosphate and α-D-galactose-1-phosphate. Rh-FGD1 accepted D-glucose as substrate, although with very low catalytic activity.

For determining the steady-state kinetic parameters with F_{420} and glucose-6-phophsate as substrate, Rh-FGD1 activity was monitored following the decrease in absorbance at 420 nm associated with the reduction of F_{420}. The kinetic data did fit well when using the Michaelis–Menten kinetic model. The kinetic parameters for the natural substrates G6P and F_{420} were determined (Table 4.3)

by keeping one of the substrates constant (F$_{420}$ at 20 µM or G6P at 2.0 mM, respectively), while varying the other substrate concentration. The apparent K_m values for G6P and F$_{420}$ are 0.31 mM and 3.8 µM, respectively. The Km value for F$_{420}$ is very similar to that observed with FGDs from Mtb (K_d = 4.5 µM) and *M. smegmatis* (4 µM) (Purwantini and Daniels 1996; Bashiri et al. 2008). The K_m value for G6P is closer to that for Mtb-FGD (0.1 mM) whereas it is much lower than the equivalent value from FGD in *M. smegmatis* (1.6 mM). The observed differences in K_m values for G6P can partly be explained by different levels of G6P in these organisms; e.g., it is known that mycobacterial cells can contain high levels of G6P (Hasan et al. 2010; Purwantini and Daniels 1996).
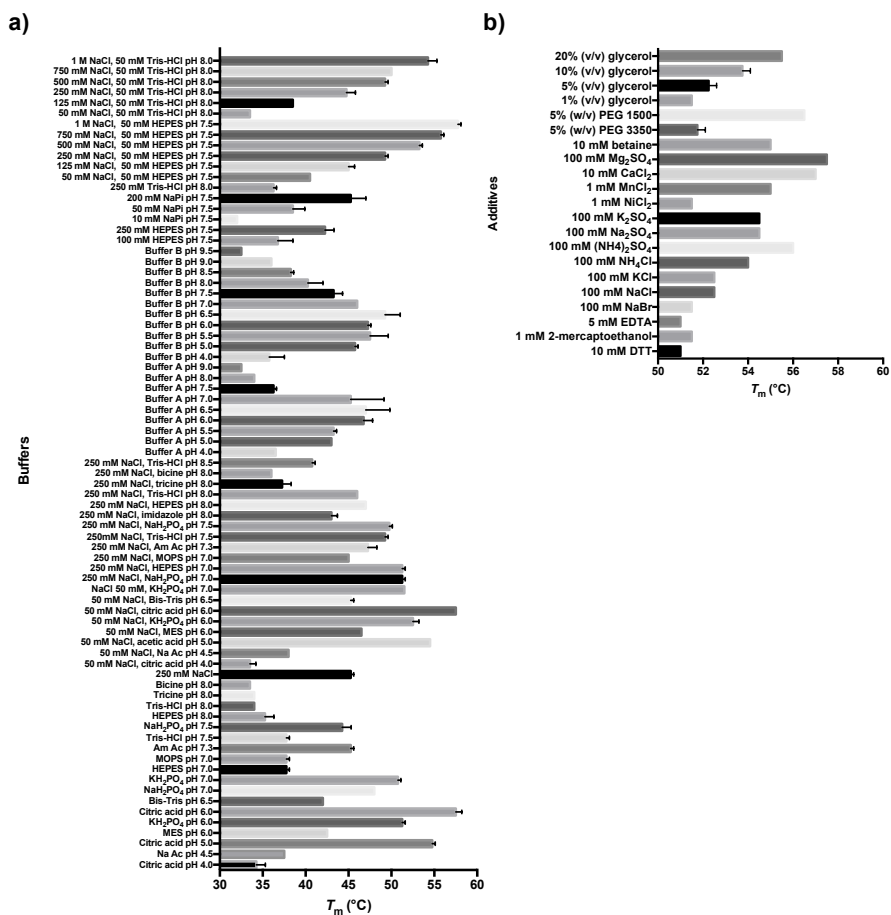
Figure 4.3: Melting temperatures of Rh-FGD1 in different buffer (**a**) and additive (**b**) conditions measured by the Thermofluor technique. Buffers were used at concentration of 100 mM unless otherwise indicated. The error bars represent SD from the three replicates. Buffer A: succinic acid/ NaH$_2$PO$_4$/ glycine = (2:7:7). Buffer B: citric acid/ CHES/ HEPES = (2:4:3). Ac: acetate, Am: ammonium, DTT: dithiothreitol.

Table 4.3: Steady-state kinetic parameters for the wild-type Rh-FGD1, K197N Rh-FGD1, K258N Rh-FGD1, and R282Q Rh-FGD1 for G6P and glucose

Rh-FGD1	glucose-6-phosphate			glucose		
	K_m [mM]	k_{cat} [s^{-1}]	k_{cat}/K_m [M^{-1} s^{-1}]	K_m [mM]	k_{cat} [s^{-1}]	k_{cat}/K_m [M^{-1} s^{-1}]
wild-type	0.31 ± 0.02	17 ± 0.32	57000	>300	>0.02	0.06
K197N	95 ± 12	3.80 ± 0.29	40	>300	>0.02	0.07
K258N	61 ± 5.1	0.57 ± 0.02	9.4	>300	>0.0009	0.004
R282Q	>100	>0.047	0.67	>300	>0.005	0.002
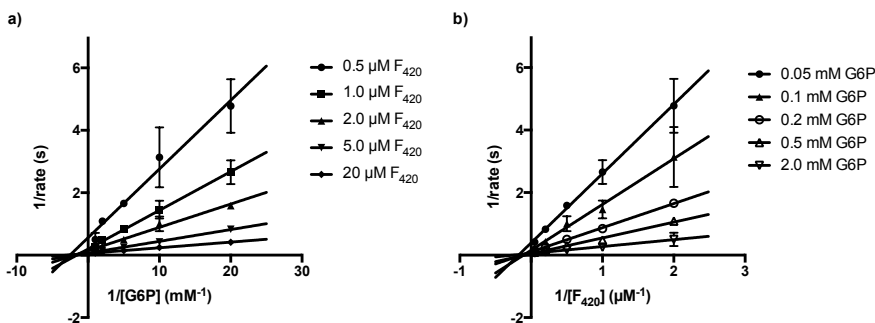
Figure 4.4: Two-substrate kinetic analysis for Rh-FGD1 via double reciprocal plots of reaction rates against (**a**) G6P or (**b**) F_{420} concentrations. These lines intercepts at one point, corresponding to the formation of a ternary complex Rh-FGD1:G6P:F_{420} to generate 6-phosphogluconolactone and $F_{420}H_2$.

As the FGD-catalyzed reaction involves two substrates, G6P and F_{420}, we set out to decipher which mechanism is operative for Rh-FGD1, namely a ping-pong, sequential or random mechanism. Both substrate concentrations were varied and the F_{420} reduction rates were measured accordingly. Increasing concentrations of both substrates G6P and F_{420} resulted in an increase in reaction rates, suggesting that the reaction occurs via a ternary complex Rh-FGD1:G6P:F_{420}. This is best illustrated by the observed intersection of the lines when double reciprocal values of the reaction rates and substrate concentrations are plotted (Figure 4.4). Whether these two substrates bind in an ordered or a random manner, however, remains to be further investigated, e.g., by product inhibition or tracer studies with radioactive labeled substrates.

4.3.4. FGD1 overall structure

The crystal structure of Rh-FGD1 was determined at 1.47 Å resolution by molecular replacement using Mtb-FGD1 devoid of all ligands (PDB ID code 3B4Y) (Bashiri et al. 2008) as the search model. The asymmetric unit contains two enzyme monomers forming a compact dimer (Figure 4.5a), which is also observed in solution as estimated by gel permeation analysis (data not shown), similarly to the mycobacterial homolog (1.0 Å rmsd difference for 610 pairs of Cα atoms)

(Figure 4.5b). The very good quality of the electron density enabled us to model several residues in a double conformation and to identify a residue with a *cis* peptide bond in proximity of the active site (Figure 4.5c). Only residues 254–263 in subunit A, and 250–279 in subunit B lack clear electron density and were therefore excluded from the final model. Each Rh-FGD1 monomer is comprised of residues 1–334, forming an $(\alpha/\beta)_8$ TIM-barrel, with the active site typically located at the C-terminus of the barrel, as observed in Mtb-FGD1 (Bashiri et al. 2008). As indicated by the Dali server (Holm and Rosenstrom 2010), this protein topology is shared also with other homologous members of the luciferase-like hydride transferase family, including a secondary alcohol dehydrogenase (Adf) and a methylene-tetrahydromethanopterin reductase (Mer) (34 and 25% sequence identity with Rh-FGD1, respectively) (Aufhammer et al. 2004; Aufhammer et al. 2005). The two Rh-FGD1 molecules present in the asymmetric unit are essentially identical, as indicated by an overall rmsd difference of 0.55 Å in Cα atomic positions of 302 residues, except for a segment comprising residues 41–49, which was excluded in the non-crystallographic symmetry restrained refinement. The dimer interface area is rather large, burying approximately 2000 Å^2 [as analyzed by the program PISA (Krissinel and Henrick 2007)] and accounting for ∼14% of the monomer's surface. Unless explicitly stated, hereafter we will refer to monomer A for describing the structure.

4.3.5. F_{420} binding site

All attempts to elucidate the structure of Rh-FGD1 in its holoenzyme form, i.e. with the F_{420} cofactor bound, were unsuccessful. Nonetheless, the obtained overall structure is substantially identical to that of the F_{420}–bound Mtb-FGD1 and the architecture of the active site is conserved. Therefore, the F_{420} molecule was tentatively modelled in the Rh-FGD1 as a result of the superposition of the mycobacterial enzyme structure (Figure 4.5b,c). In particular, the high quality electron density clearly indicates the presence of a well-ordered non-prolyl *cis*-peptide bond between Ser72–Val73 constituent of a bulge at the end of a β strand close to the presumed binding site of the F_{420} isoalloxazine ring (Figure 4.5c). This unusual *cis*-peptide is highly conserved in this enzyme family, being consistently observed in Mtb-FGD1, Adf, and Mer (joining Ser74–Val75, Cys72–Ile73 and Gly61–Val62, respectively). This bulge is essential as it serves as a backstop to hold the isoalloxazine ring from its *re*-face, bending the deazaisoalloxazine ring into a butterfly conformation (Aufhammer et al. 2005; Bashiri et al. 2008; Aufhammer et al. 2004).

The F_{420} binding pocket is largely identical among FGDs, Adf, and Mer wherein the deazaisoalloxazine ring locates at the innermost part of the pocket and the hydrophilic polyglutamate tail extends into the solvent (Figures 4.5d and 4.6). The most noticeable difference between the various structures of F_{420}-binding proteins is a helical coil region located at the C-terminus of the TIM-barrel, creating a sort of lid element that stabilizes cofactor binding (Figure 4.6). In Rh-FGD1 the sequence for this structural element is shorter than that of the homologous enzymes and corresponds to the disordered part (residues 254-263 in monomer A). The high flexibility of this region may correlate with a more dynamic interaction with the cofactor and may well explain the difficulty in ob-
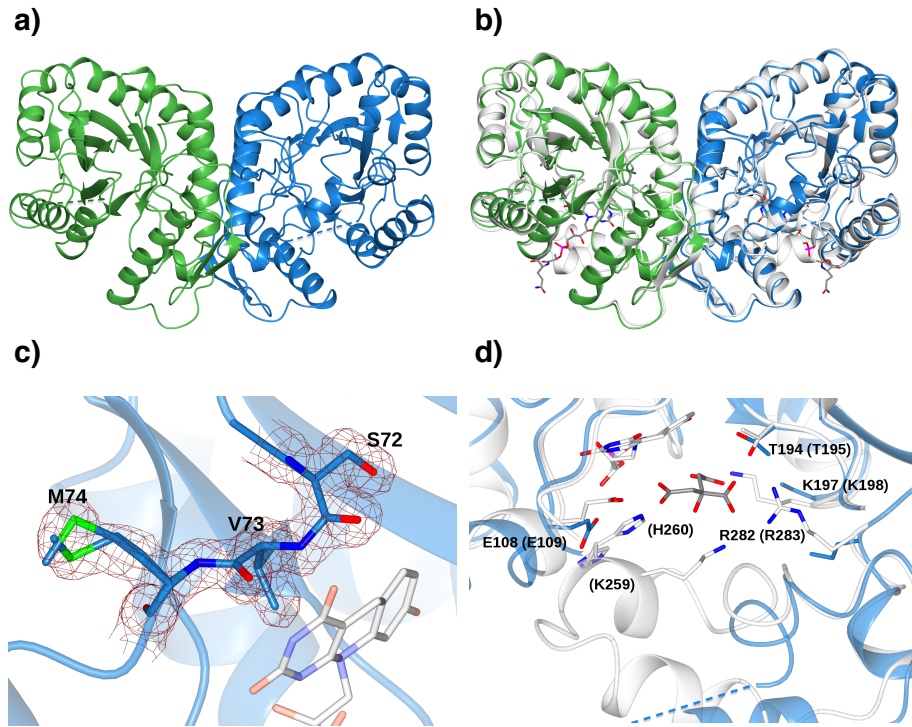
Figure 4.5: Crystal structure of Rh-FGD1 from *Rhodococcus jostii* RHA1. **a)** Ribbon diagram of the Rh-FGD1 dimer showing the $(\alpha/\beta)_8$ TIM-barrel architecture of the two monomers colored in light blue (monomer A) and green (monomer B), respectively. The disordered region in each monomer is represented by a dashed line corresponding to residues 254–263 and 250–279 in monomers A and B, respectively. **b)** Superposition of the Rh-FGD1 dimer (colored as in a) onto the homologous Mtb-FGD1 [in white, 84% sequence identity, PDB ID 3Y4B (Bashiri et al. 2008)] with its F_{420} cofactor bound (carbon, oxygen, nitrogen and phosphorus atoms in white, red, blue and magenta, respectively). **c)** The non-prolyl *cis* peptide bond (connecting Ser72 and Val73) and Met74 in a double conformation (sulfur atoms in green) are fitted to the initial $2F_o - F_c$ electron density map contoured at 1.2 σ (brown chicken-wire). As a reference, the cofactor F_{420} from the Mtb-FGD1 structure (superposed as in b) is drawn with shaded colors. **d)** Close-up of the Rh-FGD1 active site superposed to Mtb-FGD1 as in b. The Mtb-FGD1 inhibitor citrate (carbon in grey) is shown bound to the active site. Putative residues involved in substrate binding are labeled with the corresponding Mtb-FGD1 residues in parentheses. The δ, ϵ carbon and ζ nitrogen atoms of K197, and the guanidinium group of R282 side chains were not visible in the electron density and were not included in the final model.
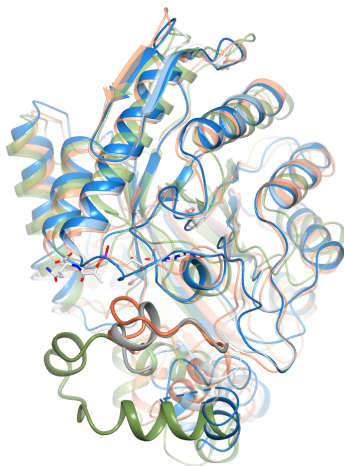
Figure 4.6: Comparison between the active site of Rh-FGD1 (blue) with that of Mtb-FGD1 (3B4Y, white), Adf (1RHC, coral), and Mer (1Z69, green). For clarity, only the F_{420} from Mtb-FGD1 is shown. The insertion regions of Mtb-FGD1, Adf, and Mer corresponding to the highly disordered segment in Rh-FGD1 (residues 254–263, represented by a dashed line) are highlighted in bold style. The orientation of the molecule is approximately 90° rotated along an axis perpendicular to the plane of the paper with respect to that in Figure 4.5c. Color coding for atoms is as in Figure 4.5b

taining the Rh-FGD1 structure in its holoenzyme form.

4.3.6. Glucose-6-phosphate binding site

In Mtb-FGD1, a citrate molecule, most likely derived from the crystallization solution, was found to bind adjacent to the F_{420} molecule and later proved to be a competitive inhibitor for Mtb-FGD1. Citrate occupies a cavity with a size that can fit G6P in an orientation suitable for catalysis. This allowed the modelling of G6P into the active site of Mtb-FGD1, revealing highly conserved residues involved in substrate binding and catalysis (Bashiri et al. 2008) (Figure 4.5d). It has been postulated that in Mtb-FGD1, the phosphate moiety of G6P occupies a positively charged pocket constituted by side chains of Lys198, Lys259, and Arg283 (Bashiri et al. 2008) (Figure 4.5b). In Rh-FGD1, out of the three residues, the position of Lys258 is unknown as it is part of the disordered region. Instead, Lys197 and Arg282 are visible and adopt a similar conformation with respect to the corresponding residue in Mtb-FGD1. Nevertheless, part of their side chains lack clear electron density (Cδ, Cε, and Nζ of the former and the guanidinium group of the latter), implying a much higher flexibility. Sequence alignment indicated that the three residues are strictly conserved in proteins exhibiting FGD activity (Bashiri et al. 2008). Rv0132c—sharing 36% sequence identity with Mtb-FGD1 and previously annotated as Mtb-FGD2—does not contain these phosphate group binding residues and consistently showed no such assigned activity (Bashiri et al. 2012). In fact, Rv0132c was later proven to be an F_{420}-dependent hydroxymycolic acid dehydrogenase and was proposed to be

an unprecedented antitubercular target that may also be inhibited by the novel drug pretomanid (PA-824) (Purwantini and Mukhopadhyay 2013).

To further probe the roles of these residues, we generated single mutations, namely K197N, K258N, and R282Q Rh-FGD1. In comparison to the wild-type Rh-FGD1, the mutants showed a drastic decrease in catalytic efficiency for G6P, as indicated by K_{m} values of two orders of magnitude higher than that of the wild-type enzyme (Table 4.3). The rate of catalysis was also considerably affected: The R282Q mutant virtually lost activity whereas the K197N and K258N mutants had a 4.5- and 30-fold lower k_{cat} value, respectively, compared with the wild-type. Disruption of the phosphate binding pocket may, to a certain extent, also affect the substrate specificity. In fact, when glucose was used as a substrate instead of G6P, the mutant K197N showed a slightly improved $k_{\mathrm{cat}}/K_{\mathrm{m}}$ when compared with the wild-type enzyme (Table 4.3). These data unequivocally verified that the three targeted residues are crucial for the binding of the phosphate moiety of the G6P. Moreover, it might become possible to improve FGD activity towards glucose, e.g., by random mutagenesis of residues forming the G6P binding pocket.

4.4. Discussion

4.4.1. Physiological role of Rh-FGDs

F_{420} is an unusual redox cofactor originally found exclusively in a restricted number of microbes, such as archaea and actinomycetes. Astonishingly, a bioinformatics study in 2010, indicated that F_{420} can be much more widespread than previously thought and present in 11% of all sequenced bacteria and archaea (Selengut and Haft 2010). In particular, *R. jostii* RHA1 was predicted to contain at least 104 deazaflavoenzymes, an impressively large number. In line with this prediction, we present here the first experimental evidence for the presence of $F_{420}H_2$-dependent enzymes in R. jostii RHA1. More specifically, the *R. jostii* RHA1 genome encodes at least three FGDs: RHA1_RS43115 (WP_011600337.1), RHA1_RS10755 (WP_011595003.1), and RHA1_RS43570 (WP_011600440.1) (referred to as Rh-FGD1, Rh-FGD2, and Rh-FGD3, respectively). We have focused our exploration on Rh-FGD1, the best expressed one, characterized the kinetic properties and elucidated the structure of the apo protein at high resolution. On a cautionary note, it should be noticed that the Rh-FGD1 and Rh-FGD3 are plasmid encoded whereas Rh-FGD2 is instead encoded by a chromosomal gene. Preliminary tests (data not shown), however, indicated that Rh-FGD1 and Rh-FGD2 have comparable specific activity. This gene redundancy is generally believed to facilitate the high catabolic versatility in rhodococci (van der Geize and Dijkhuizen 2004; McLeod et al. 2006).

F_{420}-dependent glucose-6-phosphate dehydrogenase has been suggested to be the primary enzyme responsible for the F_{420} reduction in several actinomycetal genera, including mycobacteria, thereby linking their central metabolism to the F_{420} reduction reaction (Purwantini and Daniels 1996). The main role of mycobacterial FGDs appears to be the generation of $F_{420}H_2$ as these bacilli also encode the conventional NADP$^+$-dependent glucose-6-phosphate dehydrogenases (Purwantini et al. 1997), which interestingly showed no significant phylogenetical relation to FGDs (Purwantini and Daniels 1998). A deletion of either *fgd*

4

or *fbiC*—a gene involved in the biosynthesis of F_{420}—renders these mycobacterial strains incapable of reducing xenobiotics via $F_{420}H_2$-dependent reductases (Taylor et al. 2010; Hasan et al. 2010; Stover et al. 2000; Manjunatha et al. 2006). Nevertheless, the physiological role of FGDs in *Rhodococcus* spp. remains largely unclear. It is well known that in *Rhodococcus opacus* and *Nocardioides simplex*, the reduced F_{420} is supplied mainly by F_{420}:NAPDH oxidoreductases (FNOs) rather than FGDs (Ebert et al. 1999; Heiss et al. 2002; Ebert et al. 2001; Heiss et al. 2003). FNOs were found to be expressed from the same operon as the $F_{420}H_2$-dependent hydride transferases, which are responsible for the degradation of environmental nitroaromatic compounds such as picrate and 2,4-dinitrophenols (Ebert et al. 1999; Heiss et al. 2002; Ebert et al. 2001). However, it cannot be excluded that FGDs also play a (crucial) role in generating $F_{420}H_2$. As very little is known about the natural substrates of the $F_{420}H_2$-dependent enzymes in *Rhodococcus* spp., it can be speculated that FGDs are primarily responsible for providing the reductant for the endogenous metabolism, maintaining the redox homeostasis during normal growth or in response to oxidative stress as observed in mycobacteria. Several lines of evidence have revealed the pivotal role of G6P as an electron reservoir mobilized via FGDs in protecting mycobacteria against oxidative and nitrosative stress (Hasan et al. 2010; Gurumurthy et al. 2013). In fact, the presence of a $NADP^+$-dependent glucose-6-phosphate dehydrogenase alone failed to render a *M. smegmatis* mutant deficient in FGD capable of surviving oxidative stress. Further investigations, e.g., gene deletion studies in combination with isotopic labelling metabolomics, are therefore necessary to decipher the precise role of FGDs in rhodococci (van der Geize at al. 2008).

4.4.2. FGDs as biocatalyst for cofactor regeneration

The biocatalytic reduction of F_{420} has been carried out so far with the use of Mtb-FGD1 (Manjunatha et al. 2006). Such reduced F_{420} is essential in studying deazaflavin-dependent reductases. However, mycobacterial FGDs are poorly to moderately expressed as soluble protein when *E. coli* is used as a heterologous expression host (Purwantini and Daniels 1998; Bashiri et al. 2007; Manjunatha et al. 2006). To overcome this limitation, a dedicated *M. smegmatis* expression strategy was developed to enhance the solubility of mycobacterial proteins. The typical yield obtained was 7 mg of pure recombinant Mtb-FGD1 from 1 L of *M. smegmatis* culture (Bashiri et al. 2007). In contrast, we produced soluble Rh-FGD1 in rather high yield: 80 mg of pure protein L^{-1} of culture. The developed *E. coli*-based expression system facilitates the routine production of soluble FGD which can be used for the synthesis of reduced F_{420}. Rh-FGD1 is a relatively fast enzyme, with a k_{cat} of 17 sec^{-1} for G6P (Table 4.3). In addition, Rh-FGD1 appears to be thermostable in most common buffers and additives (Figure 4.3); upon storage at −80 °C, Rh-FGD1 retained >90% activity after one year.

    The observation that Rh-FGD1 displayed some activity, yet very low (Table 4.3), with glucose, a much cheaper substrate instead of G6P, hints to the possibility to engineer Rh-FGD1 into a more efficient F_{420}-dependent glucose dehydrogenase. The first logical target for such tailoring efforts would be the phosphate binding pocket. Interestingly, when glucose was used as substrate, the mutant K197N showed an improved k_{cat}/K_m value of 30% higher than that of the wild

type. Therefore, by fine-tuning these residues by site-directed mutagenesis, one could obtain mutants with improved activity with the cheap co-substrate glucose. Given its robustness and accessibility, Rh-FGD1 represents a potential candidate for the biocatalytic reduction of F_{420} in larger scale or in fusion with other valuable $F_{420}H_2$-dependent reductases in a redox self-sufficient whole-cell biotransformation.

Acknowledgments

References

Ahmed FH, Carr PD, Lee BM, Afriat-Jurnou L, Mohamed AE, Hong N, Flanagan J, Taylor MC, Greening C, Jackson CJ (2015) Sequence–Structure–Function classification of a catalytically diverse oxidoreductase superfamily in Mycobacteria. J Mol Biol 427:3554–3571

Aufhammer SW, Warkentin E, Berk H, Shima S, Thauer RK, Ermler U (2004) Coenzyme binding in F_{420}-dependent secondary alcohol dehydrogenase, a member of the bacterial luciferase family. Structure 12:361–370

Aufhammer SW, Warkentin E, Ermler U, Hagemeier CH, Thauer RK, Shima S (2005) Crystal structure of methylenetetrahydromethanopterin reductase (Mer) in complex with coenzyme F_{420}: Architecture of the F_{420}/FMN binding site of enzymes within the nonprolyl *cis*-peptide containing bacterial luciferase family. Protein Sci 14:1840–1849

Bashiri G, Perkowski EF, Turner AP, Feltcher ME, Braunstein M, Baker EN (2012) Tat–dependent translocation of an F_{420}–binding protein of *Mycobacterium tuberculosis*. PloS One 7:e45003

Bashiri G, Rehan AM, Greenwood DR, Dickson JM, Baker EN (2010) Metabolic engineering of cofactor F_{420} production in *Mycobacterium smegmatis*. PLoS One 5:e15803

Bashiri G, Squire CJ, Baker EN, Moreland NJ (2007) Expression, purification and crystallization of native and selenomethionine labeled *Mycobacterium tuberculosis* FGD1 (Rv0407) using a *Mycobacterium smegmatis* expression system. Protein Expr Purif 54:38–44

Bashiri G, Squire CJ, Moreland NJ, Baker EN (2008) Crystal structures of $F_{420}H_2$-dependent glucose-6-phosphate dehydrogenase FGD1 involved in the activation of the anti-tuberculosis drug candidate PA-824 reveal the basis of coenzyme and substrate binding. J Biol Chem 283:17531–17541

Battye TG, Kontogiannis L, Johnson O, Powell HR, Leslie AG (2011) iMOSFLM: a new graphical interface for diffraction-image processing with MOSFLM. Acta Crystallogr D Biol Crystallogr 67:271–281

Boivin S, Kozak S, Meijers R (2013) Optimization of protein purification and characterization using Thermofluor screens. Protein Expr Purif 91:192–206

Britton HTS, Robinson RA (1931) CXCVIII.-Universal buffer solutions and the dissociation constant of veronal. J Chem Soc:1456–1462

Cheeseman P, Toms-Wood A, Wolfe RS (1972) Isolation and properties of a fluorescent compound, factor 420, from *Methanobacterium* strain M.o.H. J Bacteriol 112:527–531

Coats JH, Li GP, Kuo MS, Yurek DA (1989) Discovery, production, and biological assay of an unusual flavenoid cofactor involved in lincomycin biosynthesis. J Antibiot (Tokyo) 42:472–474

Daniels L, Bakhiet N, Harmon K (1985) Widespread distribution of a 5-deazaflavin cofactor in *Actinomyces* and related bacteria. Syst Appl Microbiol 6:12–17

4

de Poorter LM, Geerts WJ, Keltjens JT (2005) Hydrogen concentrations in methane-forming cells probed by the ratios of reduced and oxidized coenzyme F420. Microbiology 151:1697–1705

Denny WA (2015) TBA-354: A new drug for the treatment of persistent tuberculosis. Chem New Zeal 1:18–22

DiMarco AA, Bobik TA, Wolfe RS (1990) Unusual coenzymes of methanogenesis. Annu Rev Biochem 59:355–394

Ebert S, Rieger PG, Knackmuss HJ (1999) Function of coenzyme F_{420} in aerobic catabolism of 2,4,6-trinitrophenol and 2,4-dinitrophenol by *Nocardioides simplex* FJ2-1A. J Bacteriol 181:2669–2674

Ebert S, Fischer P, Knackmuss H (2001) Converging catabolism of 2,4,6-trinitrophenol (picric acid) and 2,4-dinitrophenol by *Nocardioides simplex* FJ2-1A. Biodegradation 12:367–376

Eirich LD, Vogels GD, Wolfe RS (1978) Proposed structure for coenzyme F_{420} from *Methanobacterium*. Biochemistry (NY) 17:4583–4593

Emsley P, Cowtan K (2004) Coot: model-building tools for molecular graphics. Acta Crystallogr D Biol Crystallogr 60:2126–2132

Greening C, Ahmed FH, Mohamed AE, Lee BM, Pandey G, Warden AC, Scott C, Oakeshott JG, Taylor MC, Jackson CJ (2016) Physiology, biochemistry, and applications of $F_{420}H_2$- and F_o-dependent redox reactions. Microbiol Mol Biol Rev 80:451–493

Gurumurthy M, Rao M, Mukherjee T, Rao SP, Boshoff HI, Dick T, Barry CE, Manjunatha UH (2013) A novel F_{420}-dependent anti-oxidant mechanism protects *Mycobacterium tuberculosis* against oxidative stress and bactericidal agents. Mol Microbiol 87:744–755

Hartzell PL, Zvilius G, Escalante-Semerena JC, Donnelly MI (1985) Coenzyme F_{420} dependence of the methylenetetrahydromethanopterin dehydrogenase of *Methanobacterium thermoautotrophicum*. Biochem Biophys Res Commun 133:884–890

Hasan MR, Rahman M, Jaques S, Purwantini E, Daniels L (2010) Glucose-6-phosphate accumulation in mycobacteria: implications for a novel $F_{420}H_2$-dependent anti-oxidant defense system. J Biol Chem 285:19135–19144

Heiss G, Hofmann KW, Trachtmann N, Walters DM, Rouvière P, Knackmuss H (2002) npd gene functions of *Rhodococcus* (*opacus*) *erythropolis* HL PM-1 in the initial steps of 2,4,6-trinitrophenol degradation. Microbiology 148:799–806

Heiss G, Trachtmann N, Abe Y, Takeo M, Knackmuss HJ (2003) Homologous npdGI genes in 2,4-dinitrophenol- and 4-nitrophenol-degrading *Rhodococcus* spp. Appl Environ Microbiol 69:2748–2754

Holm L, Rosenstrom P (2010) Dali server: conservation mapping in 3D. Nucleic Acids Res 38: W545–W549

Isabelle D, Simpson DR, Daniels L (2002) Large-scale production of coenzyme $F_{420}H_2$-5,6 by using *Mycobacterium smegmatis*. Appl Environ Microbiol 68:5750–5755 Jacobson F, Walsh C (1984) Properties of 7,8-didemethyl-8-hydroxy-5-deazaflavins relevant to redox coenzyme function in methanogen metabolism. Biochemistry (NY) 23:979–988

Jacobson FS, Daniels L, Fox JA, Walsh CT, Orme-Johnson WH (1982) Purification and properties of an 8-hydroxy-5-deazaflavin-reducing hydrogenase from *Methanobacterium thermoautotrophicum*. J Biol Chem 257:3385–3388

Jirapanjawat T, Ney B, Taylor MC, Warden AC, Afroze S, Russell RJ, Lee BM, Jackson CJ, Oakeshott JG, Pandey G, Greening C (2016) The redox cofactor F_{420} protects mycobacteria from diverse antimicrobial compounds and mediates a reductive detoxification system. Appl Environ Microbiol 82:6810–6818

Krissinel E, Henrick K (2007) Inference of macromolecular assemblies from crystalline state. J Mol Biol 372:774–797

Lapalikar GV, Taylor MC, Warden AC, Onagi H, Hennessy JE, Mulder RJ, Scott C, Brown SE, Russell RJ, Easton CJ (2012a) Cofactor promiscuity among $F_{420}H_2$-dependent reductases enables them to catalyse both oxidation and reduction of the same substrate. Catal Sci Technol 2:1560–1567

Lapalikar GV, Taylor MC, Warden AC, Scott C, Russell RJ, Oakeshott JG (2012b) $F_{420}H_2$-dependent degradation of aflatoxin and other furanocoumarins is widespread throughout the Actinomycetales. PLoS One 7:e30114

Li W, Chou S, Khullar A, Gerratana B (2009a) Cloning and characterization of the biosynthetic gene cluster for tomaymycin, an SJG-136 monomeric analog. Appl Environ Microbiol 75:2958–2963

Li W, Khullar A, Chou S, Sacramo A, Gerratana B (2009b) Biosynthesis of sibiromycin, a potent antitumor antibiotic. Appl Environ Microbiol 75:2869–2878

4

Manjunatha UH, Boshoff H, Dowd CS, Zhang L, Albert TJ, Norton JE, Daniels L, Dick T, Pang SS, Barry CE 3rd (2006) Identification of a nitroimidazo-oxazine-specific protein involved in PA-824 resistance in *Mycobacterium tuberculosis*. PNAS 103:431–436

Matsumoto M, Hashizume H, Tomishige T, Kawasaki M, Tsubouchi H, Sasaki H, Shimokawa Y, Komatsu M (2006) OPC-67683, a nitro-dihydro-imidazooxazole derivative with promising action against tuberculosis *in vitro* and in mice. PLoS Med 3:e466

McLeod MP, Warren RL, Hsiao WW, Araki N, Myhre M, Fernandes C, Miyazawa D, Wong W, Lillquist AL, Wang D, Dosanjh M, Hara H, Petrescu A, Morin RD, Yang G, Stott JM, Schein JE, Shin H, Smailus D, Siddiqui AS, Marra MA, Jones SJ, Holt R, Brinkman FS, Miyauchi K, Fukuda M, Davies JE, Mohn WW, Eltis LD (2006) The complete genome of *Rhodococcus* sp. RHA1 provides insights into a catabolic powerhouse. PNAS 103:15582–15587

McNicholas S, Potterton E, Wilson KS, Noble ME (2011) Presenting your structures: the CCP4mg molecular-graphics software. Acta Crystallogr D Biol Crystallogr 67:386–394

Murshudov GN, Vagin AA, Dodson EJ (1997) Refinement of macromolecular structures by the maximum-likelihood method. Acta Crystallogr D Biol Crystallogr 53:240–255

Ney B, Ahmed FH, Carere CR, Biswas A, Warden AC, Morales SE, Pandey G, Watt SJ, Oakeshott JG, Taylor MC (2016) The methanogenic redox cofactor F_{420} is widely synthesized by aerobic soil bacteria. ISME J 11:125–137

Pantoliano MW, Petrella EC, Kwasnoski JD, Lobanov VS, Myslik J, Graf E, Carver T, Asel E, Springer BA, Lane P, Salemme FR (2001) High-density miniaturized thermal shift assays as a general strategy for drug discovery. J Biomol Screen 6: 429–440

Purwantini E, Gillis TP, Daniels L (1997) Presence of $F_{420}H_2$-dependent glucose-6-phosphate dehydrogenase in *Mycobacterium* and *Nocardia* species, but absence from *Streptomyces* and *Corynebacterium* species and methanogenic archaea. FEMS Microbiol Lett 146:129–134

Purwantini E, Mukhopadhyay B (2013) Rv0132c of *Mycobacterium tuberculosis* encodes a coenzyme $F_{420}H_2$-dependent hydroxymycolic acid dehydrogenase. PloS One 8:e81985

Purwantini E, Mukhopadhyay B, Spencer RW, Daniels L (1992) Effect of temperature on the spectral properties of coenzyme F_{420} and related compounds. Anal Biochem 205:342–350

Purwantini E, Daniels L (1998) Molecular analysis of the gene encoding F_{420}-dependent glucose-6-phosphate dehydrogenase from *Mycobacterium smegmatis*. J Bacteriol 180:2212–2219

Purwantini E, Daniels L (1996) Purification of a novel coenzyme $F_{420}H_2$-dependent glucose-6-phosphate dehydrogenase from *Mycobacterium smegmatis*. J Bacteriol 178:2861–2866

Purwantini E, Mukhopadhyay B (2009) Conversion of NO_2 to NO by reduced coenzyme F_{420} protects mycobacteria from nitrosative damage. PNAS 106:6333–6338

Schrittwieser JH, Velikogne S, Kroutil W (2015) Biocatalytic imine reduction and reductive amination of ketones. Adv Synth Catal 357:1655–1685

Selengut JD, Haft DH (2010) Unexpected abundance of coenzyme $F_{420}H_2$-dependent enzymes in *Mycobacterium tuberculosis* and other actinobacteria. J Bacteriol 192:5788–5798

Singh R, Manjunatha U, Boshoff HI, Ha YH, Niyomrattanakit P, Ledwidge R, Dowd CS, Lee IY, Kim P, Zhang L, Kang S, Keller TH, Jiricek J, Barry CE, 3rd (2008) PA-824 kills nonreplicating *Mycobacterium tuberculosis* by intracellular NO release. Science 322:1392–1395

Stover CK, Warrener P, VanDevanter DR, Sherman DR, Arain TM, Langhorne MH, Anderson SW, Towell JA, Yuan Y, McMurray DN (2000) A small-molecule nitroimidazopyran drug candidate for the treatment of tuberculosis. Nature 405:962–966

Tasneen R, Williams K, Amoabeng O, Minkowski A, Mdluli KE, Upton AM, Nuermberger EL (2015) Contribution of the nitroimidazoles PA-824 and TBA-354 to the activity of novel regimens in murine models of tuberculosis. Antimicrob Agents Chemother 59:129–135

Taylor MC, Jackson CJ, Tattersall DB, French N, Peat TS, Newman J, Briggs LJ, Lapalikar GV, Campbell PM, Scott C (2010) Identification and characterization of two families of $F_{420}H_2$-dependent reductases from mycobacteria that catalyse aflatoxin degradation. Mol Microbiol 78:561–575

Taylor M, Scott C, Grogan G (2013) $F_{420}H_2$-dependent enzymes-potential for applications in biotechnology. Trends Biotechnol 31:63–64

Tzeng SF, Bryant MP, Wolfe RS (1975a) Factor 420-dependent pyridine nucleotide-linked formate metabolism of *Methanobacterium ruminantium*. J Bacteriol 121:192–196

Tzeng SF, Wolfe RS, Bryant MP (1975b) Factor 420-dependent pyridine nucleotide-linked hydrogenase system of *Methanobacterium ruminantium*. J Bacteriol 121:184–191

Vagin A, Teplyakov A (2010) Molecular replacement with MOLREP. Acta Crystallogr D Biol Crystallogr 66:22–25

4

van der Geize R, Dijkhuizen L (2004) Harnessing the catabolic diversity of rhodococci for environmental and biotechnological applications. Curr Opin Microbiol 7:255–261

van der Geize R, de Jong W, Hessels GI, Grommen AW, Jacobs AA, Dijkhuizen L (2008) A novel method to generate unmarked gene deletions in the intracellular pathogen *Rhodococcus equi* using 5-fluorocytosine conditional lethality. Nucleic Acids Res 36:e151

Vitt S, Ma K, Warkentin E, Moll J, Pierik AJ, Shima S, Ermler U (2014) The F$_{420}$H$_2$- reducing [NiFe]-hydrogenase complex from *Methanothermobacter marburgensis*, the first X-ray structure of a group 3 family member. J Mol Biol 426:2813–2826

Waddell WJ (1956) A simple ultraviolet spectrophotometric method for the determination of protein. J Lab Clin Med 48:311–314

Wang P, Bashiri G, Gao X, Sawaya MR, Tang Y (2013) Uncovering the enzymes that catalyze the final steps in oxytetracycline biosynthesis. J Am Chem Soc 135:7138–7141

Warkentin E, Mamat B, Sordel-Klippert M, Wicke M, Thauer RK, Iwata M, Iwata S, Ermler U, Shima S (2001) Structures of F$_{420}$H$_2$:NADP$^+$ oxidoreductase with and without its substrates bound. EMBO J 20:6561–6569

Winn MD, Ballard CC, Cowtan KD, Dodson EJ, Emsley P, Evans PR, Keegan RM, Krissinel EB, Leslie AG, McCoy A, McNicholas SJ, Murshudov GN, Pannu NS, Potterton EA, Powell HR, Read RJ, Vagin A, Wilson KS (2011) Overview of the CCP4 suite and current developments. Acta Crystallogr D Biol Crystallogr 67:235–242

Wood GE, Haydock AK, Leigh JA (2003) Function and regulation of the formate dehydrogenase genes of the methanogenic archaeon *Methanococcus maripaludis*. J Bacteriol 185:2548–2554

4